

Electronic and magnetic effects of a stacking fault in cobalt nanoscale islands on the Ag(111) surfaceKeiji Doi,¹ Emi Minamitani,^{2,*} Shunji Yamamoto,¹ Ryuichi Arafune,³ Yasuo Yoshida,^{1,†}
Satoshi Watanabe,² and Yukio Hasegawa¹¹*The Institute for Solid State Physics, The University of Tokyo, Kashiwa 277-8581, Japan*²*Department of Materials Engineering, The University of Tokyo, Tokyo 113-8656, Japan*³*International Center for Materials Nanoarchitectonics (WPI-MANA), National Institute for Materials Science, Tsukuba 304-0044, Japan*

(Received 10 February 2015; published 24 August 2015)

By utilizing spin-polarized scanning tunneling microscopy (STM) and spectroscopy, we observe the coexistence of perpendicularly and in-plane magnetized cobalt nanoscale islands on an Ag(111) surface. The magnetization direction has the relationship with the observed moiré-corrugation amplitude on the islands; the islands with stronger moiré corrugation show perpendicular magnetization, and the ones with weaker moiré corrugation exhibit in-plane magnetization. We calculate the magnetic anisotropy energy for various stackings of a Co nanostructure based on density functional theory, and we reveal that perpendicular magnetic anisotropy is reduced drastically with increasing fcc stacking faults in the Co layer. Simulated STM images reproduce the moiré-corrugation difference observed experimentally when the stacking difference between perpendicularly and in-plane magnetized islands is considered. These theoretical analyses strongly suggest that the electronic and magnetic differences between the two types of islands are caused by the presence of fcc stacking faults in the intrinsic hcp stacking of Co.

DOI: [10.1103/PhysRevB.92.064421](https://doi.org/10.1103/PhysRevB.92.064421)

PACS number(s): 75.75.-c, 68.37.Ef, 71.15.Mb, 75.25.-j

I. INTRODUCTION

Magnetic thin films with perpendicular magnetic anisotropy (PMA) have attracted considerable attention in the last decade from the viewpoint of technological applications such as high-density magnetic storage [1], magnetic random access memory [2], and other spintronics applications [3]. Cobalt (Co), a 3d transition metal, is a typical material for experimental studies of PMA in magnetic nanoscale structures because it has several advantageous properties: strong uniaxial magnetic anisotropy and the ability to control its properties in various shapes such as single atoms [4–6], nanoscale islands [7–10], and thin films [11,12]. There are reports on the emergence of PMA of Co single atoms on Pt(111) [4,5] and MgO thin films [6], and also on that of Co nanoscale structures formed on noble metals [7–12]. In particular, nanosized Co clusters or islands are attractive for ultrahigh-density magnetic-recording applications [13,14] and, therefore, it is important to identify and characterize factors that may be detrimental to such applications. One of the factors that drastically reduce the magnetic anisotropy is stacking faults in intrinsic hcp structures [15–17]. However, we are not thus far aware of any experimental efforts to investigate the effects microscopically at an atomically controlled level.

In this study, we performed microscopic investigations of the electronic and magnetic properties of Co nanoscale islands on a Ag(111) substrate by using a combination of spin-polarized scanning tunneling microscopy (SPSTM) experiments and density functional theory (DFT) calculations. Cobalt islands with triangular or hexagonal shapes and thicknesses ranging from five to eight monolayers (MLs) were grown on the substrate. The islands were found to exhibit a moiré pattern. The islands were categorized into two groups with respect to the corrugation amplitude of the pattern in STM

topographic images taken at -0.2 V as islands with stronger and weaker moiré-corrugation amplitudes. Via nanoscale magnetometry based on SPSTM, we found that the islands with stronger moiré corrugation exhibit hysteretic magnetization curves with perpendicular magnetizations while the ones with weaker moiré corrugation exhibit in-plane magnetization without hysteresis. By calculating the magnetic anisotropies of the islands, we figured out that the magnetocrystalline anisotropy of the Co nanoislands, which favors perpendicular magnetization, is significantly reduced due to the presence of a fcc stacking fault in an intrinsic hcp structure. Upon increasing the number of stacking faults to two, the magnetocrystalline anisotropy becomes weaker than the shape anisotropy of the islands, which favors in-plane magnetization, thus resulting in a variation in the easy-magnetization axis from perpendicular to in-plane. Calculations of the integrated local density of states (LDOS) reproduced the observed moiré contrasts, which indicates that the difference in the moiré-corrugation amplitude arises from the difference in the stacking structure; the pure hcp and the structures with a single fcc stacking fault, or the ones with more than two stacking faults. This result strongly suggests that the effect of an fcc stacking fault on the intrinsic hcp structure plays an important role in determining the electronic and magnetic properties of the Co nanoscale structures.

II. EXPERIMENTAL DETAILS

All measurements were performed in a low-temperature ultrahigh-vacuum STM (Unisoku USM-1300S with RHK controller R9). The sample and the tip can be cooled with liquid He, and an external magnetic field can be applied perpendicular to the sample surface. For the detection of spin-dependent tunneling current, we used a bulk Cr tip [18–21] that was electrochemically etched from a Cr rod. The tip was made of the antiferromagnetic material and minimizes stray fields which may modify the magnetic properties of samples. In our

*eminamitani@cello.t.u-tokyo.ac.jp

†Corresponding author: yyoshida@issp.u-tokyo.ac.jp

SPSTM measurements, the tip exhibited weak perpendicular magnetization whose direction can be flipped by an external magnetic field. This is probably due to the presence of a Co nanocluster picked up on the tip apex. The tip magnetization was characterized by obtaining the hysteresis curve of the spin-polarized tunneling conductance in the magnetic field [22]. For differential conductance (dI/dV) spectroscopy, we used a lock-in technique with a modulated sample bias voltage of 10 mV_{RMS} at 842 Hz. A two-dimensional dI/dV mapping was acquired simultaneously with the topographic image at a modulation voltage of 50 mV_{RMS}.

The Co/Ag(111) sample was prepared by first cleaning the substrate using a standard method: repetitive Ar sputtering and annealing at ~ 1000 K, and then depositing approximately 1 ML of Co (99.99% purity) on it by means of electron bombardment heating. The deposition rate was set to ~ 0.1 ML/s, and during the deposition the sample was kept at room temperature.

III. EXPERIMENTAL RESULTS

Figure 1(a) shows a typical STM image of the Co-deposited Ag(111) surface at 5 K under ultrahigh-vacuum conditions. Co islands with threefold symmetric shapes and thicknesses ranging from 5 to 7 MLs are observed. Since Co has an intrinsic hcp structure, these shapes suggest that the island surface has a close-packed plane, and the island grows along the [0001] orientation. We can also easily observe a corrugation on the surfaces that are oriented along the triangular or hexagonal edges of the islands, which corresponds to the atomic row direction. The periodicity of the corrugation is 1.74 nm, which is consistent with a previous report of 3-ML-Co islands on Ag(111) [23]. The periodic corrugation is explained as a moiré pattern arising from lattice mismatch between the Co overlayer and the Ag(111) substrate [23], whose interatomic distances are 0.251 and 0.289 nm, respectively. In the pattern, eight Co atoms are situated on seven Ag atoms (seven atomic spacings of Co match to six atomic spacings of Ag) and the average interatomic distance of Co in the moiré is estimated to be 0.248 nm, which is smaller than the bulk interatomic distance [23]. Unlike the case of double-layer Co on Cu(111) [24–26], the periodicity does not change with bias voltage, thus ruling out the possibility that the corrugation is due to surface standing waves.

The most interesting observation here is that islands have different moiré-corrugation amplitudes at the sample bias voltage of -0.2 V; some of the islands exhibit a larger moiré corrugation than the others. We observed both upward- and downward-pointing triangular islands; this directional variation implies their different stacking at the interface between the islands and the substrate. However, it is clear from the image that this interfacial stacking difference does not affect the moiré-corrugation amplitude since some of the triangular islands point to the same direction while exhibiting different moiré-corrugation amplitudes. Therefore, the interfacial stacking difference is not the origin of the moiré difference. To compare the difference in the moiré-corrugation amplitudes we focus on two Co islands with 6-ML thicknesses, which are shown in Fig. 1(b). The right-hand-side island in Fig. 1(b) has a larger moiré-corrugation amplitude (height

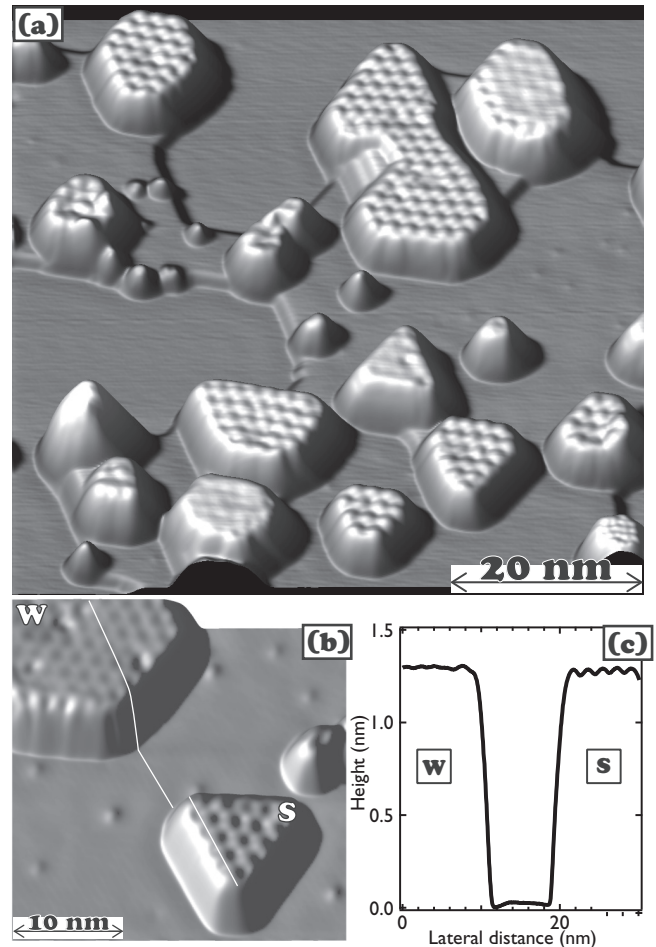


FIG. 1. (a) Overview image of Co-deposited Ag(111) surface (sample bias voltage $V_S = -0.2$ V, tunneling current $I_T = 1$ nA). Co islands with thicknesses ranging from 5 to 7 MLs are observed. (b) Constant-current image of the 6-ML Co islands on Ag(111) ($V_S = -0.2$ V, $I_T = 0.5$ nA). The island types are labeled with S (strong moiré) and W (weak moiré). (c) Cross-sectional profile as indicated in panel (b), along the two islands that has the same thickness. S and W indicate the island types.

modulation: 25 pm) than the one on the left (8 pm), as clearly shown by the corresponding cross-sectional profile in Fig. 1(c).

In order to clarify the origin of the corrugation difference, we investigated the electronic structures of the two types of islands by means of spin-averaged dI/dV spectroscopy. In the previous work [23], the protrusion and two hollow sites in the moiré structure are identified as the sites where interfacial Co atoms are located on the top, hcp, and fcc sites of Ag(111), and referred as α , β , and γ sites, respectively. Distinct dI/dV spectra are reported for the three different sites of islands with more than three atomic layers [23]. In our measurements, we first measured spectra at the three positions in the moiré structure, protrusion and two hollow sites [see inset of Fig. 2(a)], of islands with stronger moiré corrugation. We compared the acquired spectra to those at the three different sites of 3-ML islands reported in the previous work. We could easily find one-to-one correspondence of the three positions in the moiré structure between the two works because of similarities in the spectra. We determined the three

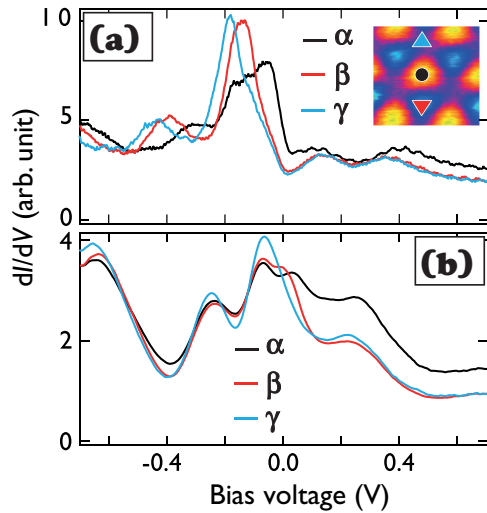


FIG. 2. (Color online) Spin-averaged dI/dV spectra obtained at three different sites (α , β , γ) in the moiré pattern on the (a) strong- and (b) weak-moiré-patterned islands. The tip-sample separation was stabilized with the setting of $I_T = 1.0$ nA and $V_S = -0.7$ V. Inset of panel (a) is the corresponding STM image (3.1 nm \times 3.1 nm, $I_T = 1.0$ nA and $V_S = -0.2$ V) showing the exact positions of α (black circle), β (red triangle), and γ (blue triangle) sites.

sites (α , β , and γ) of islands with stronger moiré corrugation based on the correspondence. Then, we determined the sites of the islands with weaker moiré corrugation according to the relative positions of the sites determined for the islands with stronger moiré corrugation on the same surface.

In the spectra acquired from islands with stronger moiré-corrugation amplitudes [Fig. 2(a)], two distinct peaks are observed below the Fermi energy (E_F) for all sites. The peak positions vary significantly depending on the sites. At the α site, a large peak appears around -0.1 V with a shoulder at around -0.2 V followed by a small peak at -0.3 V. At the β (γ) site, the large peak appears sharper than that at the α site at -0.15 V (-0.2 V) and the small peak appears at -0.4 V (-0.45 V). In contrast, on islands with weaker moiré-corrugation amplitudes these peaks are correspondingly shifted to -0.08 V and -0.25 V and appear at almost the same energies for all sites. Since the contrast in constant-current STM images depends on the integral of LDOS between E_F and the set bias voltage, variations in the

peak positions around the voltage affect the STM contrast. We thus conclude that the difference in the moiré-corrugation amplitude between the islands observed in STM topographies at $V_S = -0.2$ V is due to the difference in the electronic structures. Hereafter in this paper, we refer to the islands of interest as strong- or weak-moiré islands with respect to the moiré-corrugation amplitudes in the STM topographies at $V_S = -0.2$ V. These kinds of distinct peaks below E_F originate from the minority- and majority-spin d bands in the case of Co/Cu(111), which has been previously confirmed via comparison of the dI/dV spectra with the calculated LDOS [24,27]. A similar assignment was also performed for the current system by Gopakumar *et al.*; the -0.2 V (-0.4 V) peak of the strong-moiré island was ascribed to the minority (majority) spin state [23].

To investigate the magnetic properties of the moiré islands and their responses to external magnetic fields, we utilized the SPSTM technique with a perpendicularly magnetized Cr bulk tip [18–21]. First, we investigated strong-moiré islands by obtaining dI/dV mappings at -0.4 V, which corresponds to the voltage at which the majority-spin channel is located. The topographic STM image shown in the leftmost panel of Fig. 3 has both strong- and weak-moiré islands, which are labeled as S and W, respectively. The thickness of the islands ranges from 6 to 8 ML. The three images on the right show the dI/dV mappings obtained at a voltage of -0.4 V for at the perpendicular magnetic fields of -0.5 , -0.1 , and -0.26 T (in the downward field sweep). We can easily observe changes in the dI/dV contrast of the strong-moiré islands (labeled A to D) in the three images. The dI/dV values of four strong-moiré islands in Fig. 3 measured in various magnetic fields are plotted in Fig. 4, together with those acquired for the weak-moiré island labeled E, which does not exhibit contrast variation. The absence of the spin contrast on island E is simply because of the absence of spin states at the bias voltage. The absence is not because of hydrogen contamination or the segregation of substrate atoms onto the surface unlike the case of Co/Cu(111) [29–31], since the weak-moiré islands also show dI/dV contrast variation at different bias voltages, as will be shown later in Fig. 6(a).

The butterfly shape of the curves obtained for islands A to D is a magnetoresistance curve that is typically obtained in magnetic tunneling junctions [32–34], and it has also been reported in SPSTM studies [35,36]. The shape can be explained as a consequence of the flippings of the magnetization directions

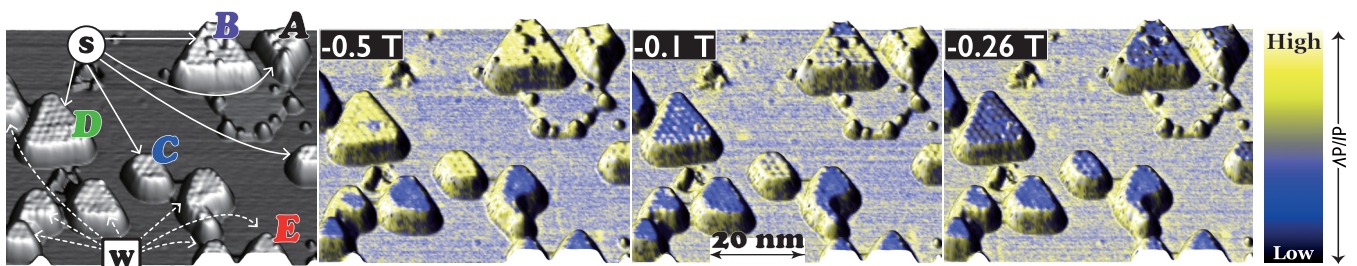


FIG. 3. (Color online) Topography (leftmost panel) and spin-resolved dI/dV colorized topographies at magnetic fields of -0.5 , -0.1 , and -0.26 T (in the downward field sweep) ($V_S = -0.4$ V, $I_T = 1$ nA). A more detailed field dependence of the dI/dV mapping is available as a movie [28]. The island types are labeled S (strong moiré) and W (weak moiré) in the topography. The thicknesses of the islands are A: 7 MLs, B: 8 MLs, C: 6 MLs, D: 6 MLs, E: 6 MLs.

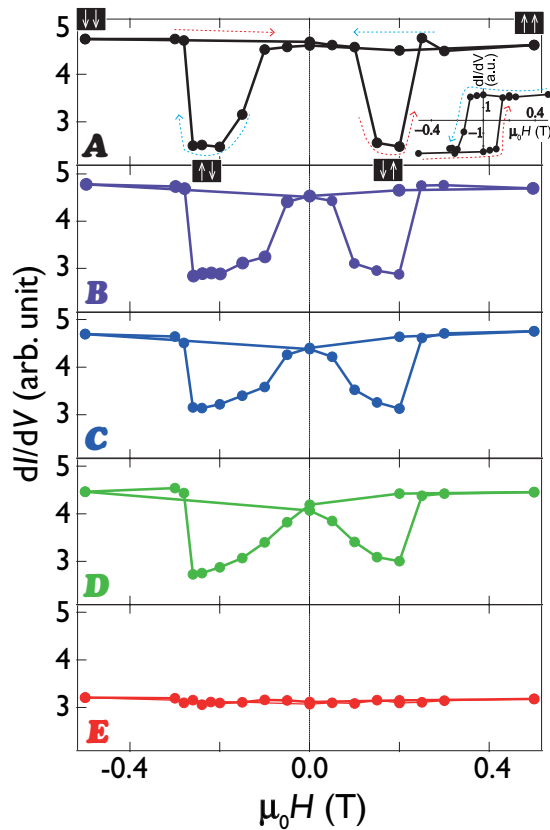


FIG. 4. (Color online) Magnetic-field dependencies of the dI/dV values corresponding to islands A to E in the spin-resolved dI/dV images shown in Fig. 3 ($V_S = -0.4$ V, $I_T = 1$ nA). The magnetic field is applied perpendicular to the surface. A butterfly shaped curve was obtained on strong moiré islands A to D but not on the weak-moiré island E. The inset of the top panel is the hysteretic dI/dV curve of island A estimated from the butterfly shaped curve given the flippings of the tip magnetization direction at -0.28 and 0.25 T.

of both the tip and the sample during the field sweep. Since all the curves exhibit abrupt changes at magnetic-field values of -0.28 and $+0.25$ T, we attribute the changes to flipping of the tip magnetization. Given the tip magnetization flipping, we can estimate the curves of the islands themselves by subtracting the contribution of the bulk Cr tip from the butterfly curves. The inset of Fig. 4 shows the magnetization curve of island A, which exhibits the typical shape of a ferromagnetic hysteresis curve. The other strong-moiré islands also exhibit similar hysteresis curves with slightly different coercivities depending on the island size and thickness. From these results, we conclude that the strong-moiré islands have ferromagnetic properties with PMA.

Spin-resolved dI/dV spectra were acquired from a strong-moiré island at fields where the tip and sample magnetizations were in parallel and antiparallel configurations, as shown in Fig. 5(a) with solid and open circles, respectively. The spectra at all sites and all configurations exhibit peaks at the same energy positions as in the case of the spin-averaged spectra [Fig. 2(a)]. In addition, the intensities vary between the parallel and antiparallel configurations. The large peak

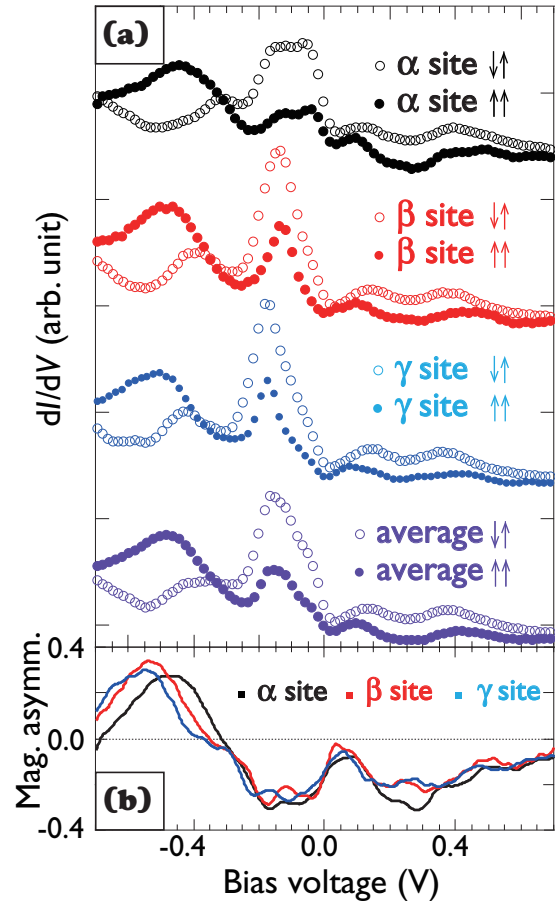


FIG. 5. (Color online) (a) Spin-resolved dI/dV spectra taken on three different sites of a strong-moiré island and their averages. Arrows $\uparrow\uparrow$ ($\uparrow\downarrow$) refer to parallel (antiparallel) configurations of the tip and sample magnetizations. The spectra with the parallel and antiparallel configurations were obtained at 1 and 0.15 T (in the downward field sweep), respectively. The tip-sample separation is stabilized with $I_T = 1.0$ nA and $V_S = -0.7$ V. (b) Magnetic asymmetries arising from opposite magnetization configurations [$A = (\uparrow\uparrow - \uparrow\downarrow) / (\uparrow\uparrow + \uparrow\downarrow)$] at the three different sites.

close to E_F is enhanced for the antiparallel configuration, while the small peak around -0.45 V is enhanced for the parallel configuration [7,23]. From the spectra, we estimated the magnetic asymmetry for each site [Fig. 5(b)]. The overall trends are similar for all sites; however, a clear shift in energy for the majority-spin state is observed between α and the other sites, thereby indicating that the spin-polarization of the Co island is spatially modulated by the moiré structure, similar to the case of Co nanoislands on Cu(111) where the spin-polarization is modulated by standing waves [26].

Next, we focus on the magnetic properties of the weak-moiré islands. The variation of the dI/dV obtained from the spin-resolved dI/dV mappings at -0.2 V on the weak-moiré island [inset of Fig. 6(a)] at various magnetic fields is plotted in Fig. 6(a). The slope changes at around ± 0.25 T most likely correspond to the flippings of the tip magnetization, as observed in Fig. 4. The linear features up to -1.0 T suggest that the field was applied perpendicular to the easy axis of the magnetization direction and that the magnetization

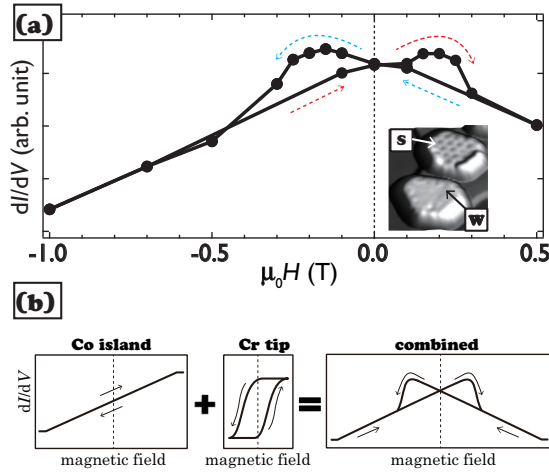


FIG. 6. (Color online) (a) Variation in the differential conductance dI/dV at -0.2 V as a function of magnetic field as acquired for the weak-moiré island (6 MLs) shown in the STM image (inset, 19 nm \times 22 nm, $V_S = -0.2$ V, $I_T = 1$ nA). The magnetic field was applied perpendicular to the surface plane. (b) Schematic showing the decomposition of the shape of the curve in panel (a). The experimental data are qualitatively explained as a combination of the magnetization curves of the in-plane-magnetized Co island and the perpendicularly magnetized tip in perpendicular magnetic fields.

was not saturated even beyond the saturation fields of the strong-moiré islands (≤ 0.3 T). Therefore, the overall features can be attributed to a combination of the linear magnetization curve of the Co island and the hysteresis curve of the Cr bulk tip, as described schematically in Fig. 6(b). Since we applied magnetic fields perpendicular to the surface, this observation strongly suggests that the island is magnetized parallel to the surface. These observations reveal the coexistence of perpendicularly and in-plane-magnetized Co islands on the same surface. A recent surface-magneto-optical-Kerr-effect study also implied the possible coexistence of the in-plane and perpendicular magnetizations on the same system but the corresponding spatial information was not reported [37]. The present results underline importance of local nanoscale structures on the overall magnetic properties and the powerful versatility of SPSTM for elucidating such issues.

IV. THEORETICAL CALCULATION

DFT calculations were performed with the use of the plane-wave-based Vienna *Ab initio* Simulation Package (VASP) [38,39] with the projected augmented wave (PAW) method [40]. The exchange and correlation were described at the level of the generalized gradient approximation (GGA). For the exchange-correlation functional, we used that determined by Perdew–Burke–Ernzerhof [41].

For the structural relaxation of free-standing five-atomic-layer Co with (1×1) periodicity, we set the energy cutoff at 400 eV and used a $15 \times 15 \times 1$ k -point mesh, and the positions of atoms in the Co layers were optimized without any constraint until the forces on individual atoms were less than 0.01 eV/atom. In the magnetocrystalline anisotropy calculation of the system, we set the cutoff energy at 600 eV and

used a $31 \times 31 \times 1$ Monkhorst–Pack k -point mesh [42]. We verified the convergence of the magnetocrystalline anisotropy energy on the cutoff energy and the k -point sampling, and we determined that the above-mentioned settings are sufficient to ensure convergence. The magnetic anisotropy energy (MAE) of the magnetocrystalline anisotropy was estimated from the difference between the total energy for the c axis (perpendicular) and that for the a axis (in-plane) magnetizations.

The Co nanoislands on Ag(111) were modeled by the slab model consisting of five-layer Co of (7×7) periodicity on a five-layer Ag(111) substrate of (6×6) periodicity and a vacuum layer of thickness of ~ 18 Å along the surface normal. During the structural optimization, the positions of atoms in the Co layers and the top four layers of the Ag(111) slab were optimized without any constraint until the forces on individual atoms were less than 0.02 eV/atom. For this system, we set the energy cutoff for the plane-wave basis at 400 eV, and the Brillouin zone was sampled with a k point only at the Γ point because of the large size of the supercell.

V. THEORETICAL ANALYSIS AND DISCUSSIONS

To understand the experimental observations, we performed theoretical calculations. It is well known that fcc-stacked Co ultrathin films grown on a Cu(100) substrate exhibit ferromagnetic properties with in-plane magnetic anisotropy [43], so we speculated that the observed differences in the moiré-corrugation amplitude and in the magnetization direction are due to differences in the layer stackings of the Co islands. First of all, we calculated the magnetocrystalline magnetic anisotropy for various stackings of free-standing 5-ML Co layers. The MAE of magnetocrystalline anisotropy due to the spin-orbit coupling was estimated by DFT calculations after structural optimization.

From Table I, we note that all stackings possess perpendicular anisotropy although the magnitude of MAE varies. Interestingly, we found that the more fcc stacking faults the Co thin film has, the less the perpendicular MAE becomes. The hcp structure (ABABA) has the strongest perpendicular anisotropy, and if we add a fcc stacking fault to this structure (ABA|CA or AB|CBC), the anisotropy value is reduced by about 15% or 20%. By adding another fcc stacking fault, a reduction of 60% with respect to that the hcp is seen for the pseudo-hcp (AB|CB|A) structure. Further addition of a fcc stacking fault yields an anisotropy reduction of about 70% for the fcc structure (AB|C|A|B). These results are reasonable in comparison with an experimental report on a Co-based alloy in which 10% of fcc stacking faults reduces the PMA by a factor of about two revealed by in-plane x-ray diffraction and magnetization measurements [15]. We also calculated the dependence of MAE on the lattice constant for two stacking structures (hcp, pseudo-hcp) as a representative of high- and low-PMA cases. We determined that changes in MAE is small for a lattice constant variation of 0.002 nm (Table II).

In addition to the magnetocrystalline magnetic anisotropy, the shape anisotropy due to the magnetic dipole interaction plays an important role in determining the magnetic anisotropy of the nanoscale structures. In low-dimensional systems such as the nanoislands considered in this study, the shape anisotropy favors in-plane magnetization and competes

TABLE I. Tabulation of the relationship between stacking structure, number of fcc stacking faults, structural stability, MAE, and shape anisotropy of free-standing 5-ML Co. The vertical bar (|) within the stacking sequences indicates a stacking fault. The structural stability and magnetic anisotropy energies were estimated per Co atom.

Stacking	Number of stacking faults	Structural stability (meV/atom)	MAE of magnetocrystalline anisotropy (meV/atom)	Shape anisotropy (meV/atom)
ABABA (hcp)	0	0	0.084	0.068
ABA CA	1	0.0131	0.064	0.069
AB CBC	1	4.95	0.071	0.069
AB CB A (pseudo-hcp)	2	7.76	0.034	0.071
AB C A B (fcc)	3	12.6	0.020	0.071

with the perpendicular magnetic anisotropy due to magnetocrystalline magnetic anisotropy. We estimated the shape anisotropy in the framework of a rotationally symmetric ellipsoid model with a magnetic moment in each structure as estimated from DFT calculations. These calculation results are summarized in Table I. By comparing these calculated values with the magnetocrystalline anisotropies, we found that in-plane magnetization is favorable for fcc and pseudo-hcp structures, while perpendicular magnetization is favorable for hcp. In the case of structures with a single fcc stacking fault (ABA|CA and AB|CBC), the two anisotropy energies are comparable within the range of our analyses, and therefore the favorable magnetization directions are not clear.

We next focus on the three stacking structures of hcp, fcc, and pseudo-hcp (one perpendicularly magnetized structure and two in-plane magnetized ones) in order to examine the possibility that the stacking difference is ascribed to the observed moiré-corrugation difference. We performed the DFT calculation corresponding to these three different staking arrangements of 5-ML Co layers formed on 5-ML Ag(111). After structural optimization, we found that the hcp structure is energetically most favorable and the fcc and pseudohcp have higher energies but are sufficiently stable to be formed in the case of room-temperature deposition: the energy difference from the hcp structure ΔE is 9.62 meV/atom for fcc and is 7.24 meV/atom for pseudo-hcp. Although we did not perform slab calculations with the Ag(111) layer for the structures with a single fcc stacking fault (ABA|CA and AB|CBC), we can easily speculate that these structures are more stable than pseudo-hcp or fcc because the number of stacking faults mainly contributes to enhancement of the total energy in the case of free-standing 5-ML Co, as can be understood from Table I. Figure 7 shows the simulated STM images based on the Tersoff–Hamann approximation for the hcp, fcc, and pseudo-hcp structures at sample bias of -0.2 eV and at the

tip position ~ 0.27 nm above the surface. The 2×2 supercells of the moiré pattern are shown here. All the structures exhibit a moiré pattern similar to that observed in the experiments from the point of view of the shape and periodicity. However, the moiré contrast amplitude is quite different between hcp and the other two structures; hcp shows a strong contrast, but fcc and pseudo-hcp exhibit considerably weaker ones. Judging from the structural stability and the moiré contrast together with the magnetization direction estimated in Table I, we conclude that the two experimentally observed types of Co islands correspond to pure hcp and structures with a single fcc stacking fault and the ones with more than two stacking faults.

Actually, based on our conclusion, we can reasonably explain the behaviors of the magnetizations of the Co islands observed in the SPSTM experiments. The perpendicularly magnetized islands shown in Fig. 4 have fairly small coercivities of $H_C \sim 0.15$ T when compared with that of bulk Co or other Co nanostructures of similar size; for instance, Co nanoscale islands on the Cu(111) surface exhibit a coercivity of $H_C \sim 1.5$ T [36]. This can be due to the weak perpendicular magnetic anisotropies of the islands caused by strong competition between magnetocrystalline and shape anisotropies in pure hcp and structures with a single fcc stacking fault (Table I). The island dependence of the coercivity and shape of the hysteresis curve (Fig. 4) might be also affected by this competition. On the other hand, the in-plane-magnetized islands do not show saturation of magnetization up to -1 T (Fig. 6), thereby indicating that the coercivity is fairly large compared to those of perpendicularly magnetized islands. This speculation is also reasonable if we assume that these islands have structures with more than two stacking faults (Table I), which have strong in-plane anisotropies.

TABLE II. Tabulation of the dependence of MAE of magnetocrystalline magnetic anisotropy on the lattice constant for two stacking structures: hcp and pseudo-hcp.

Stacking	MAE (meV)		
	0.250 nm	0.251 nm	0.252 nm
ABABA (hcp)	0.084	0.089	0.095
AB CB A (pseudo-hcp)	0.034	0.031	0.029

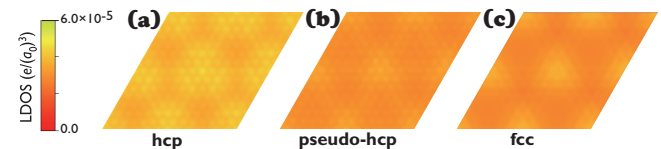


FIG. 7. (Color online) Local density of states integrated between -0.2 eV and E_F in a plane parallel to the surface, which is ~ 0.27 nm above the surface, for (a) hcp with ABABA stacking, (b) pseudo-hcp with AB|CB|A stacking, and (c) fcc with AB|C|A|B stacking. a_0 represents the Bohr radius. The 2×2 supercells of the moiré pattern are shown.

VI. CONCLUSIONS

In summary, we examined the electronic and magnetic influences of a fcc stacking fault in hcp Co nanoscale islands on the Ag(111) surface via SPSTM experiments and DFT calculations. We observed Co nanoscale islands with strong- and weak-moiré-corrugation amplitudes at $V_S = -0.2$ V. The spin-averaged dI/dV spectra indicate that the islands have different electronic structures depending on the moiré-corrugation amplitudes. The spin-polarized dI/dV images of the islands and the magnetic-field dependence clarify that islands with stronger moiré-corrugation amplitudes are perpendicularly magnetized and the ones with weaker moiré-corrugation amplitudes are magnetized in plane. Theoretical calculations explain the two types of islands with respect to the magnetic anisotropy and the moiré-corrugation amplitude by considering different stacking structures for the layers; the pure hcp and the structures with a single fcc stacking fault, and the ones with more than two stacking faults. Our results strongly suggest that the effect of fcc stacking faults

in an intrinsic hcp stacking is significant from both the electronic and magnetic points of view. These results provide important microscopic information from the perspective of the design and construction of future ultrahigh-density magnetic recording devices based on Co or Co-based alloys.

ACKNOWLEDGMENTS

We thank Christian Henneken for technical information about preparing a Cr bulk tip. We also thank Kirsten von Bergmann, Susumu Shiraki, Howon Kim, Stefan Blügel, Yoshio Miura, and Tatsuya Kawae for fruitful discussions. This work was supported by JSPS KAKENHI Grants No. 21360018, No. 23840008, No. 25110008, No. 25286055, No. 25707025, No. 25871114, No. 26120508, No. 26110507 and, also by Foundation of Advanced Technology Institute, Japan. The calculations were performed on the computer facilities of the Institute of Solid State Physics (ISSP Super Computer Center, University of Tokyo), Numerical Materials Simulator at NIMS, and RIKEN Integrated Cluster of Clusters (RICC).

-
- [1] A. Moser, K. Takano, D. T. Margulies, M. Albrecht, Y. Sonobe, Y. Ikeda, S. Sun, and E. E. Fullerton, *J. Phys. D: Appl. Phys.* **35**, R157 (2002); C. Chappert, A. Fert, and F. N. Van Dau, *Nat. Mater.* **6**, 813 (2007).
- [2] R. Sbiaa, H. Meng, and S. N. Piramanayagam, *Phys. Status Solidi RRL* **5**, 413 (2011).
- [3] S. Ikeda, K. Miura, H. Yamamoto, K. Mizunuma, H. D. Gan, M. Endo, S. Kanai, J. Hayakawa, F. Matsukura, and H. Ohno, *Nat. Mater.* **9**, 721 (2010).
- [4] P. Gambardella, A. Dallmeyer, K. Maiti, M. Malagoli, W. Eberhardt, K. Kern, and C. Carbone, *Nature (London)* **416**, 301 (2002).
- [5] P. Gambardella, S. Rusponi, M. Veronese, S. Dhési, C. Grazioli, A. Dallmeyer, I. Cabria, R. Zeller, P. Dederichs, K. Kern, C. Carbone, and H. Brune, *Science* **300**, 1130 (2003).
- [6] I. G. Rau, S. Baumann, S. Rusponi, F. Donati, S. Stepanow, L. Gragnaniello, J. Dreiser, C. Piamonteze, F. Nolting, S. Gangopadhyay, O. R. Albertini, R. M. Macfarlane, C. P. Lutz, B. A. Jones, P. Gambardella, A. J. Heinrich, and H. Brune, *Science* **344**, 988 (2014).
- [7] O. Pietzsch, A. Kubetzka, M. Bode, and R. Wiesendanger, *Phys. Rev. Lett.* **92**, 057202 (2004).
- [8] F. Meier, K. von Bergmann, P. Ferriani, J. Wiebe, M. Bode, K. Hashimoto, S. Heinze, and R. Wiesendanger, *Phys. Rev. B* **74**, 195411 (2006).
- [9] J. E. Bickel, F. Meier, J. Brede, A. Kubetzka, K. von Bergmann, and R. Wiesendanger, *Phys. Rev. B* **84**, 054454 (2011).
- [10] K. Schouteden, K. Lauwaet, D. A. Muzychenko, P. Lievens, and C. Van Haesendonck, *New J. Phys.* **13**, 033030 (2011).
- [11] M. Wasniowska, W. Wulfhchel, M. Przybylski, and J. Kirschner, *Phys. Rev. B* **78**, 035405 (2008).
- [12] H. Tokano, H. Yanagihara, and Eiji Kita, *J. Appl. Phys.* **97**, 016103 (2005).
- [13] D. Weller, A. Moser, L. Folks, M. E. Best, W. Lee, M. F. Toney, M. Schwickert, J.-U. Thiele, and M. F. Doerner, *IEEE Trans. Magn.* **36**, 10 (2000).
- [14] G. A. Prinz, *Science* **282**, 1660 (1998).
- [15] S. Hinata, R. Yanagisawa, S. Saito, and M. Takahashi, *J. Appl. Phys.* **105**, 07B718 (2009).
- [16] V. Sokalski, D. E. Laughlin, and J.-G. Zhu, *J. Appl. Phys.* **110**, 093919 (2011).
- [17] C. J. Aas, L. Szunyogh, R. F. L. Evans, and R. W. Chantrell, *J. Phys.* **25**, 296006 (2013).
- [18] A. Schlenhoff, S. Krause, G. Herzog, and R. Wiesendanger, *Appl. Phys. Lett.* **97**, 083104 (2010).
- [19] M. Corbetta, S. Ouazi, J. Borme, Y. Nahas, F. Donati, H. Oka, S. Wedekind, D. Sander, and J. Kirschner, *Jpn. J. Appl. Phys., Part 1* **51**, 030208 (2012).
- [20] N. Romming, C. Henneken, M. Menzel, J. E. Bickel, B. Wolter, K. von Bergmann, A. Kubetzka, and R. Wiesendanger, *Science* **341**, 636 (2013).
- [21] A. L. Bassi, C. S. Casari, D. Cattaneo, F. Donati, S. Foglio, M. Passoni, and C. E. Bottani, *Appl. Phys. Lett.* **91**, 173120 (2007).
- [22] G. Rodary, S. Wedekind, H. Oka, D. Sander, and J. Kirschner, *Appl. Phys. Lett.* **95**, 152513 (2009).
- [23] T. G. Gopakumar, N. Néel, J. Kröger, and R. Berndt, *Chem. Phys. Lett.* **484**, 59 (2009).
- [24] L. Diekhöner, M. A. Schneider, A. N. Baranov, V. S. Stepanyuk, P. Bruno, and K. Kern, *Phys. Rev. Lett.* **90**, 236801 (2003).
- [25] O. Pietzsch, S. Okatov, A. Kubetzka, M. Bode, S. Heinze, A. Lichtenstein, and R. Wiesendanger, *Phys. Rev. Lett.* **96**, 237203 (2006).
- [26] H. Oka, P. A. Ignatiev, S. Wedekind, G. Rodary, L. Niebergall, V. S. Stepanyuk, D. Sander, and J. Kirschner, *Science* **327**, 843 (2010).
- [27] M. V. Rastei, B. Heinrich, L. Limot, P. A. Ignatiev, V. S. Stepanyuk, P. Bruno, and J. P. Bucher, *Phys. Rev. Lett.* **99**, 246102 (2007).
- [28] See Supplemental Material at <http://link.aps.org/supplemental/10.1103/PhysRevB.92.064421> for the detailed field dependence of the dI/dV mapping of Co nanoscale islands.
- [29] M. Sicot, O. Kurnosikov, H. J. M. Swagten, and B. Koopmans, *Surf. Sci.* **602**, 3667 (2008).

- [30] P.-J. Hsu, C.-I. Lu, S.-W. Chen, W.-J. Hsueh, Y.-H. Chu, C.-H. Hsu, C. J. Butler, and M.-T. Lin, *Appl. Phys. Lett.* **96**, 142515 (2010).
- [31] A. Rabe, N. Memmel, A. Steltenpohl, and Th. Fauster, *Phys. Rev. Lett.* **73**, 2728 (1994).
- [32] J. S. Moodera, L. R. Kinder, T. M. Wong, and R. Meservey, *Phys. Rev. Lett.* **74**, 3273 (1995).
- [33] W. J. Gallagher, S. S. P. Parkin, Y. Lu, X. P. Bian, A. Marley, K. P. Roche, R. A. Altman, S. A. Rishton, C. Jahnes, T. M. Shaw, and G. Xiao, *J. Appl. Phys.* **81**, 3741 (1997).
- [34] S. Yuasa, T. Sato, E. Tamura, Y. Suzuki, H. Yamamori, K. Ando, and T. Katayama, *Europhys. Lett.* **52**, 344 (2000).
- [35] O. Pietzsch, A. Kubetzka, M. Bode, and R. Wiesendanger, *Science* **292**, 2053 (2001).
- [36] S. Ouazi, S. Wedekind, G. Rodary, H. Oka, D. Sander, and J. Kirschner, *Phys. Rev. Lett.* **108**, 107206 (2012).
- [37] Y. Saisyu, T. Hirahara, R. Hobara, and S. Hasegawa, *J. Appl. Phys.* **110**, 053902 (2011).
- [38] G. Kresse and J. Furthmüller, *Phys. Rev. B* **54**, 11169 (1996).
- [39] G. Kresse and J. Furthmüller, *Comput. Mater. Sci.* **6**, 15 (1996).
- [40] P. E. Blöchl, *Phys. Rev. B* **50**, 17953 (1994).
- [41] J. P. Perdew, K. Burke, and M. Ernzerhof, *Phys. Rev. Lett.* **77**, 3865 (1996).
- [42] H. J. Monkhorst and J. D. Pack, *Phys. Rev. B* **13**, 5188 (1976).
- [43] D. Kerkmann, *Appl. Phys. A* **49**, 523 (1989).